Journal of
Materials Chemistry B

Accepted Manuscript

This article can be cited before page numbers have been issued, to do this please use: H. Ma, M. Yang, C. Zhang, Y. Ma, Y. Qin, Z. Lei, L. Chang, L. Lei, T. Wang and Y. Yang, *J. Mater. Chem. B*, 2017, DOI: 10.1039/C7TB02399E.

ROYAL SOCIETY OF CHEMISTRY

rsc.li/materials-b

View Article Online
DOI: 10.1039/C7TB02399E

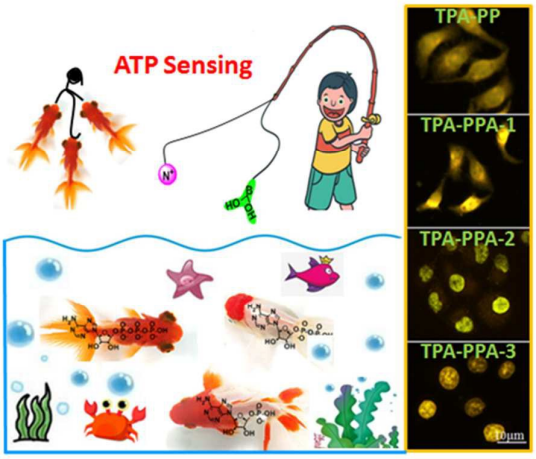

A set of novel AIE-active fluorescence probes containing pyridiniums and boric acid groups with the applications of ATP recognition and specific tracing of different cell organelle!

Journal Name

View Article Online
DOI: 10.1039/C7TB02399E

ARTICLE

Aggregation-Induced Emission (AIE)-Active Fluorescent Probes with Multi-Binding Sites toward ATP Sensing and the Live Cell Imaging

Received 00th January 20xx,
Accepted 00th January 20xx

DOI: 10.1039/x0xx00000x

www.rsc.org/

Hengchang Ma,*[a] Manyi Yang,[a] Caili Zhang,[b] Yucheng Ma,[a] Yanfang Qin,[a] Ziqiang Lei,*[a] Lu Chang,[a] Lei Lei,[a] Tao Wang,[a] Yuan Yang[a]

Aggregation-induced emission (AIE)-active compounds are attractive fluorescent materials for applications in chemical and biological sensing. That effect of such materials amplifies changes in the fluorescence signal due to the physical states transformation from aggregation to disaggregation, which can be employed for detecting various analytes with high sensitivity. Especially, the specific bio-active analytes recognition is a very interesting but also a challenging work. In this paper, we report a set of novel AIE-active fluorescence probes containing pyridiniums and boricacid groups (**TPA-PP**, **TPA-PPA-1**, **TPA-PPA-2**, **TPA-PPA-3**), which has been developed for adenosine 5'-triphosphate (ATP) recognition. These probes with two type interaction modes and multiple connection sites toward ATP molecules are able to selectively discriminate ATP among other bioactive anions with a significant enhancement in fluorescence emission. Especially, in the application of cell imaging, with the amount of positive charges and boric acid group increase further and further, probes can penetrate into cells, then enrich into nucleus very specifically. These results clearly demonstrated that the newly developed sensors are suitable for specific tracing of different cell organelle with a high visualized solution and retention ability. Therefore, all of them are confirmed as a promising alternative for live cell imaging in the future.

Introduction

Adenosine triphosphate (ATP), a fundamental biomolecule, is shared by almost all independently living organisms.[1] As the molecular unit of currency, ATP is the primary energy source for cellular processes.[2] ATP also functions as a signalling molecule for regulating cell movement, neurotransmission, and ion channels.[3] Importantly, it is incorporated into nucleic acids by polymerases during DNA replication and transcription.[4] Therefore, it is very necessary to develop new chemosensors with high selectivity and sensitivity for the detection ATP, and to further elucidate its contributions to physiological states.[5] Recently, several genetically encoded or aptamer-based fluorescent ATP probes have been developed.[6] However, it is still a compelling need to discriminate a certain nucleoside triphosphate among various nucleoside triphosphates, such as ATP, adenosine diphosphate (ADP), monophosphate (AMP).[7] Due to the ease of operation and low cost, small-molecule probes have demonstrated great application potentials in the ATP discrimination and cell imaging.[8] Then, such fluorescent ATP probes, mainly based on complexation with NH hydrogen bond,[9] positively charged cations,[10] metal ion center[11] and π–π interaction,[12] have been developed. However, owing to the challenges in overcoming issues of selectivity and response concentration, only a few ATP sensors have been applied for cell imaging.[13]

Generally, it is easy to find that cationic molecules can bind strongly with ATP through electrostatic attractions, providing fluorescent signal output, where as various probes with simple structures cannot induce specific changes due to the relative weak interactions between analytes and ATP chains, resulting in the weak optical outputs. In this work, we describe a novel boric acid group modification cationic probe for ATP recognition. To improve the sensitivity of the sensors, the synthetic proposal (Scheme 1) are designed according to the following rationales that (1) As we previously reported that the connections of triphenylamine-pyridinium are able to make the materials with intense fluorescence in the visible region because of forming electron donating and accepting systems.[14] (2) The pyridinium groups can serve as electrostatic acceptors to ATP anions,[15] and (3) importantly, boric acid groups have a specific combination towards cis-diols.[16] This design is successful and it is found that probes with multi-binding sites can cooperatively recognize ATP from other bioactive anions

[a] Key Laboratory of Eco-Environment-Related Polymer Materials Ministry of Education, College of Chemistry and Chemical Engineering, Northwest Normal University, Lanzhou, 730070 (China), E-mail: mahczju@hotmail.com (Ma HC); leizq@nwnu.edu.cn (Lei ZQ)
[b] No.99 Lianyungang Road，Rizhao Shandong，276826 (China)
† Footnotes relating to the title and/or authors should appear here.
Electronic Supplementary Information (ESI) available: [details of any supplementary information available should be included here]. See DOI: 10.1039/x0xx00000x

very selectively with a low detection limit (0.3 ppm). The cell imaging experiments were also carried out by incubation with HepG-2 liver cancer cells, these results exhibited interestingly that probes with different positive charges and boric acid groups are of excellent cell membrane permeability, but different imaging targets.

Results and discussion

Synthesis of TPA-PP, TPA-PPA-1, TPA-PPA-2 and TPA-PPA-3

Using the brominated triphenylamine (TPA) and diphenylamine (DPA) as the starting materials, then pyridin-4-ylboronic acid applied as cross-coupling partners produces the intermediate of pyridins modificated TPAs. Finally, boric acid groups substituted and unsubstituted benzyl bromides incorporated to the above prepared intermediates, leading to the formation of desirable probes **TPA-PPA-1**, **TPA-PPA-2**, **TPA-PPA-3** and a control probe of **TPA-PP** (Scheme 1, Figure 1) with excellent yields. Their structures were confirmed by ^{1}H and ^{13}C NMR. (Figure S1, S2, S3, S4. ESI†)

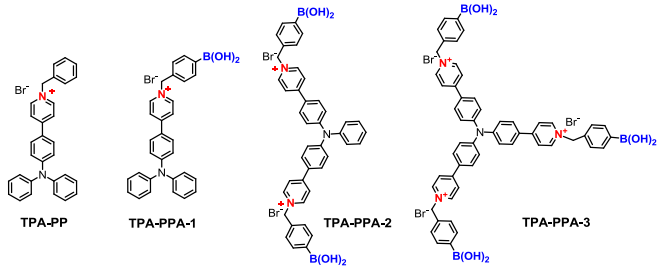

Scheme 1 Chemical structures of **TPA-PP**, **TPA-PPA-1**, **TPA-PPA-2** and **TPA-PPA-3**.

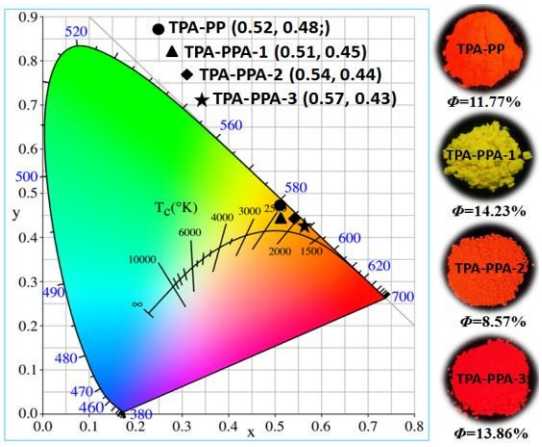

Fig. 1 Left: CIE chromaticity diagram of **TPA-PP**, **TPA-PPA-1**, **TPA-PPA-2**, **TPA-PPA-3.** Right: The corresponding Photographs and fluorescence quantum yield. (The fluorescence quantum yields were collected at the excitation wavelengths as 427, 432, 437, and 451 nm, respectively, and each emission spectrum was collected from 500 to 750 nm with 0.5 nm step and 100 ms dwell time.)

Theoretical calculations

Theoretical calculation using OPT/FREQ/B3LYP/6-31G* level in the Gaussian 09 program is carried out to characterize the three-dimensional structures and the frontier molecular orbital energy levels of all of probes. As illustrated in Figure 2, they exhibits the three-dimensional propeller structure with a very narrow energy gap of 0.09379, 0.09317, 0.03443 and 0.02856 eV. The HOMO orbital is mostly dominated in the TPA cores, and LUMO orbital mainly extends across the other electron accepting pyridinium,[17] which indicates that probes have obvious intramolecular charge transfer (ICT) tendency.

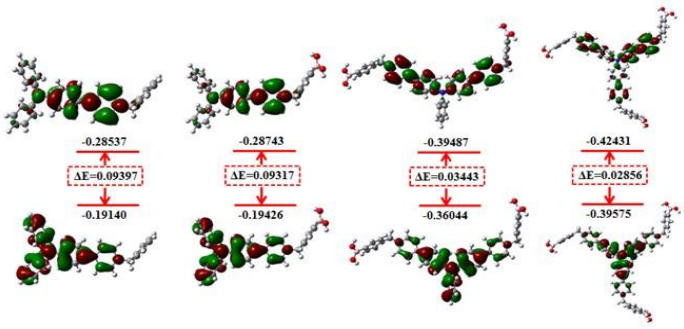

Fig. 2 Optimized molecular orbital amplitude plots of HOMO and LUMO energy levels of **TPA-PP**, **TPA-PPA-1**, **TPA-PPA-2**, **TPA-PPA-3**.

Spectroscopic studies

The emission study of probes in different solvents indicated that the fluorescence property is greatly affected by the solvent polarity, which is probably due to the intramolecular charge transfer (ICT) property.[18] In the solvent of THF, the emission bands of four probes are narrow into a more sharp peak, which is located at a long-wavelength of 610 nm approximately. Otherwise, in the case of **TPA-PPA-3**, very colorful emission performances could be seen. Especially, in the protonic solvent of MeOH, EtOH, high emission intensity and a small blue-shift occurred. Therefore, in our cases, we can conclude that the introduction of boronic acid groups and positive charges award the materials very interesting emission behaviors.

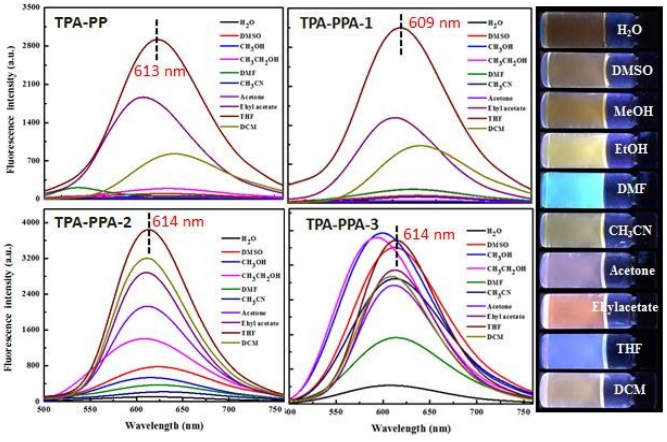

Fig. 3 The Fluorescence spectra of **TPA-PP** (λ_{ex} = 427 nm), **TPA-PPA-1** (λ_{ex} = 432 nm), **TPA-PPA-2** (λ_{ex} = 437 nm), **TPA-PPA-3** (λ_{ex} = 451 nm) at 20 μM in different solutions. Inset: The corresponding color photograph of **TPA-PPA-3** taken under illumination at 365 nm.

Apart from the time-averaging processes of the steady-state spectra measurements, time-resolved PL spectra can offer

more valuable information. Therefore, to better understand the fluorescence mechanism, the time-resolved PL decay of these probes at different conditions was studied. Figure 4 shown the PL decay curves of **TPA-PP**, **TPA-PPA-1**, **TPA-PPA-2** and **TPA-PPA-3**, their fluorescence lifetimes were lengthened to 4.9, 2.9, 4.3 and 4.9 nanoseconds, respectively. It was clear from our observation that the life time of the probes in this study are significantly longer than most organic fluorophores.[19] Their long lifetimes make these probes particularly appealing for the visualization of cellular processes in time-resolved confocal measurements, which can eliminate unwanted interfering background for high-sensitivity assays.

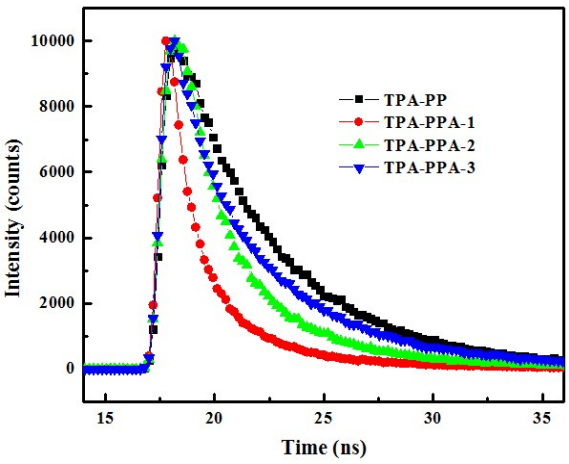

Fig. 4 Time-resolved fluorescence decays of **TPA-PP**, **TPA-PPA-1**, **TPA-PPA-2** and **TPA-PPA-3**.

ATP recognition and AIE study

The ability of **TPA-PP**, **TPA-PPA-1**, **TPA-PPA-2** and **TPA-PPA-3** to recognize ATP was investigated by absorption and fluorescence spectroscopy in aqueous solution containing 2 vol % DMSO (20 μM, pH = 7.0). (Figure S7, S8. ESI†) First of all, all Probes exhibited weak intramolecular charge transfer emission at 595-600 nm, which may be attributed to hydrogen bonding or proximity-induced quenching by aqueous molecules.[20] Upon the addition of different amounts of ATP from 10 to 300 μM, the fluorescence emission of probes were enhanced with different I/I_0 ratio. And also, a decreased absorption bands at λ = 425-450 nm were observed upon the titration of ATP These changes in emission and absorption verified that an obvious interaction takes place between probes and the ATP molecule, which is possibly due to the synergistic effect of electrostaticat traction and covalent bonds formation as we discussed above. For this consideration, we took a comparison between the control probe of **TPA-PP** and **TPA-PPA-1**. Obviously, after binding with the ATP anion, both of probes displayed the enhanced emissions, but different intensity values could be obtained. From this value, we were able to concern that boric acid groups can act as an effective partner to promote the ability toward ATP molecules recognition. Therefore, the synergistic effect definitely happened during the sensing process. What should be noted that compare to the previous reported studies, our probes possess two type interaction modes, and also, multiple connection site. Especially, in the case of **TPA-PPA-3**, this effect facilitated the recognition process very sensitive and so quick. Compare to **TPA-PPA-1**, while addition of 300 μM ATP to the solution of **TPA-PPA-3**, which led to an almost 6-fold turn-on response. Meanwhile, from the titration video (video: Specific selective titration experiment, ESI†), we can see that the instantaneous emission enhancement occurs after adding the ATP solution to the **TPA-PPA-3** aqueous phase. Furthermore, the linear range of **TPA-PPA-3** for ATP detection was found at very low concentrations from 0.3 to 1.0 ppm, suggesting a detection limit of 0.3 ppm (Figure S9, ESI†). This implies that probe **TPA-PPA-3** can quantitatively detect ATP at very low levels. From Table 1, we found the fluorescence quantum yield of probe is enhanced greatly after charging 200 μM ATP. Especially, in the case of **TPA-PPA-3**, the fluorescence quantum yield was improved almost as much as 26-folds. Therefore, we can conclude that our probes take advantages of very sensitive sensing ability toward ATP molecules.

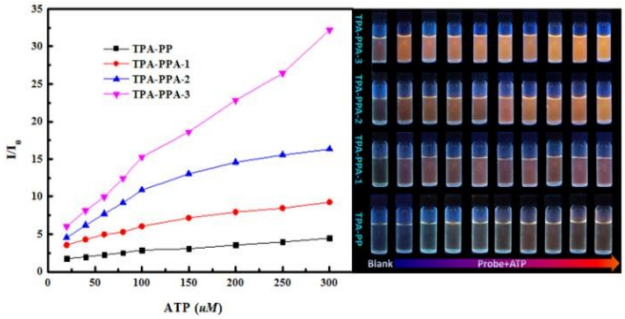

Fig. 5 Left: Plots of maximum emission intensity (I/I_0) of **TPA-PP**, **TPA-PPA-1**, **TPA-PPA-2**, **TPA-PPA-3** with the addition of ATP. Right: The corresponding photographs taken under illumination at 365 nm.

In the following research program, we are very anxious to make a clear understanding of the ATP sensing mechanism. As previous documents and our findings reported that triphenylamine derivatives are typically AIE-active compounds.[21] It was also well know that AIE-active materials are sensitive to the changes of environmental viscosity, which is reasonably due to the restriction of intramolecular rotations (RIR), blocking the non-radiative pathway and opening up the radiative channel.[22] As a result, AIE molecules become more emissive in the higher viscosity conditions. Therefore, this fluorescence property of **TPA-PPA-3** was screened in the mixture of MeOH-Glycerol with different fractions to adjust solvent viscosity. As the solvent of glycerol is charged into MeOH from 0 to 95 vol%, the viscosity is promoted gradually, and the fluorescence enhancement of **TPA-PPA-3** also could be achieved almost 5-folds with less than 5 nm blue-shift when the glycerol-MeOH ratio is maintained at 0.95 (Figure 6). The elevated emission behavior verified the AIE property of **TPA-PPA-3**. Thus, we postulated that the ATP sensing process involves the multiple sites binding formation between ATP and **TPA-PPA-3**. Reasonably, more binding site formed, then more viscous the reaction media was, and also, more intramolecular rotations were restricted. Finally, more emissive the probe was.

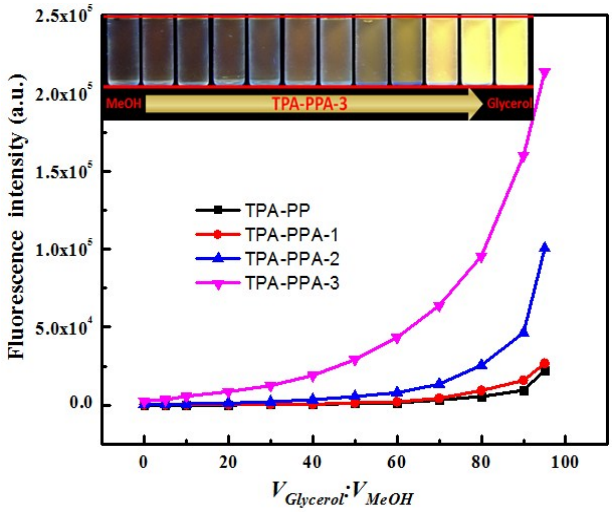

Fig. 6 Plots of maximum emission intensity of **TPA-PP**, **TPA-PPA-1**, **TPA-PPA-2**, **TPA-PPA-3** with the $V_{Glycerol}$: V_{MeOH} *from 0 to 0.95* (Conc.: 20 µM, Inset shown the images of **TPA-PPA-3** in the mixture of Glycerol & MeOH ($V_{Glycerol}$: V_{MeOH} = 0 to 0.95) taken under illumination at 365 nm.

To address the molecular mechanism beyond this observation, the influence of the nucleotides those bear different numbers of phosphate groups were examined. The changes in the fluorescence spectra of **TPA-PPA-3** in aqueous phase upon adding biologically important anions such as ADP, AMP, as well as halide ions and various phosphate ions. As shown in Figure 7, very noticeable selectivity to the ATP response could be detected, it was also found that the emission spectrum of TPA-PPA-3 changed negligibly upon the addition of ADP, AMP, and other anions, which means that **TPA-PPA-3** shows a high selectivity towards ATP over a number of tested anions, which includes several other phosphates.

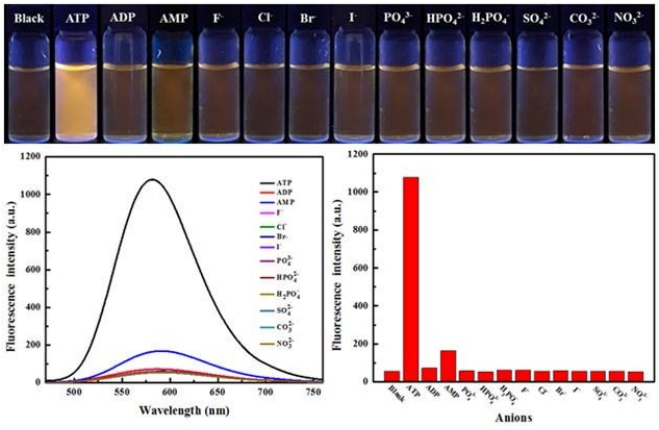

Fig. 7 Fluorescence spectra of **TPA-PPA-3** (λ_{ex} = 451 nm, 20 µM) upon the addition of ATP, ADP, AMP (100 µM) and other anions (100 µM) in aqueous solution containing 2 vol% DMSO. The corresponding bar graph and color photograph.

Cell cytotoxicity assessment and cellular imaging applications

Finally, the cytotoxicity and biological imaging of **TPA-PP**, **TPA-PPA-1**, **TPA-PPA-2** and **TPA-PPA-3** in cultured cells were investigated. The MTT assay was carried out for HepG-2 liver cancer cells to study their cytotoxic tolerance towards these probes.[23] The results showed that more than 85% cells are viable after 24 h of incubation of HepG-2 cells with probe **TPA-PP**, **TPA-PPA-1**, **TPA-PPA-2** and **TPA-PPA-3** in the concentration range of 0-50 µg/mL, which indicated that all of probes are only slightly toxic towards cells within this concentration window. (Figure S10, ESI†) Figure 8 shown the fluorescence image of HepG-2 cells incubated with probes (working conc.: 20 ug/mL) for 30 min at temperature of 37 °C. The bright fluorescence images were observed inside the cells, indicating that all probes successfully penetrate the cell membrane and enrich into specific cell organelles under physiological conditions, which might come from the positive charges of the pyridinium moieties and the target-specific interactions between probes and biomoleculues.

In the case of the control probe **TPA-PP** and **TPA-PPA-1**, whole cell morphology could be seen. To confirm the specificity of these AIE-active probes, DAPI, a commercially available and typical fluorescent dye for nuclear staining, was used as a calibration to stain the cell nucleus. From the co-staining experiments Figure 9, we can see that **TPA-PP** and **TPA-PPA-1** are most located at cell cytoplasm. However, with the amount of positive charges and boricacid groups increase further (following the order of **TPA-PPA-1**, **TPA-PPA-2** and **TPA-PPA-3**), the cellular uptake and distribution profiles were so different, probes can penetrate into cells, then enriched into nucleus very specifically. The co-staining experiments clearly demonstrated that the orange fluorescence from **TPA-PPA-3** has an excellent overlap with the blue emission of DAPI. Therefore, **TPA-PPA-3** was definitely a cell nucleus targeted probe with a high visualized solution and retention ability with minimum background staining. Compare to the high toxic and expensive commercially available DAPI, **TPA-PPA-3** was confirmed as a promising alternative for nucleus-specific live cell imaging in the future.

From these research points, we can hard to say that these new developed sensors are exactly ATP-specific in the mammalian cells. The positive charges were definitely play important role for sensors to permeate and enter into the different cell organelle. Then, the interactions between sensors with bio-analytes occurred, resulting in the specific cell organelle imaging. This study is ongoing in our lab.

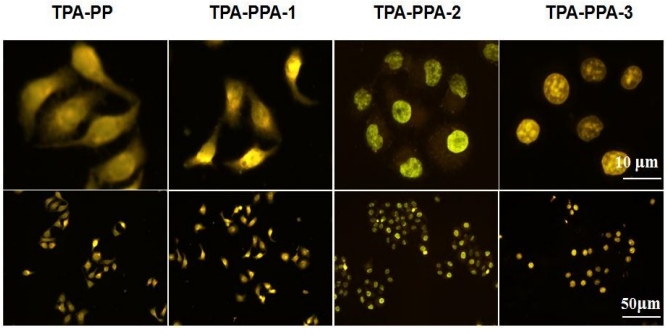

Fig. 8 Fluorescence micrographs of HeGP-2 cells stained with 20 µg/mL **TPA-PP**, **TPA-PPA-1**, **TPA-PPA-2**, **TPA-PPA-3** for 60 min in different magnifications.

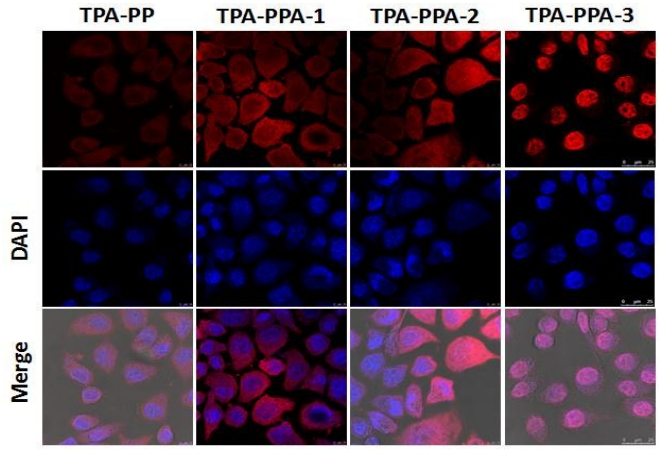

Fig. 9 Co-staining of **TPA-PP**, **TPA-PPA-1**, **TPA-PPA-2**, **TPA-PPA-3** with nucleus-specific dye DAPI and the overlay images.

Conclusions

In conclusion, we have designed and synthesized a new set of AIE-active fluorescence probes containing triphenylamine core and cationic pyridinium and boricacid groups. (**TPA-PP**, **TPA-PPA-1**, **TPA-PPA-2**, **TPA-PPA-3**) These probes were able to respond to ATP discrimination among other bioactive anions with a different enhancement in fluorescence emission. Especially, due to the presence of two type interaction modes, and multiple connection site, **TPA-PPA-3** can facilitate the ATP recognition process very sensitive (detection limit: 0.3 ppm) and so quick. In the application of cell imaging, these probes bearing the same triphenylamine core and a different amount of positive charges and boricacid groups, but displayed very different imaging world. Our research result may provide new concept of cellular tracker designing and make an insight into biological questions, understanding disease mechanism. Our research is on-going along this line.

Experimental section

General procedures. 4-bromotriphenylamine (99%), tris(4-iodophenyl)amine (98%), pyridine-4- boronic acid (99%), tetrakis(triphenylphosphine)palladium(0) ($Pb(PPh_3)_4$ 98%), potassium carbonate (K_2CO_3, 99%), bis(4-bromophenyl)amine, (99%), iodobenzene (98%), benzyl bromide (98%), 4-bromomethylphenylboronic acid (98%)， 1,10-Phenanthroline (99%),adenosine 5'-triphosphate (ATP) sodium salt, adenosine 5'-diphosphate (ADP) sodium salt and adenosine 5'-monophosphate (AMP) sodium salt were purchased from Aladdin Co. Nitrogen with a purity of 99.99% was provided from commercial source. Other reagents, such as N, N-dimethylformamide (DMF), toluene, dichloromethane (DCM), methanol, ethanol, tetrahydrofuran (THF), ethyl acetate, chloroform, and was purchased from Energy Chemical Company.

Characterization. ^1H NMR (600 MHz), ^{13}C NMR (150 MHz) spectra was recorded on MERCURY spectrometer at 25 °C, and all NMR spectra were referenced to the solvent. UV-visible absorption spectra (UV) were recorded on a PU-1901spectromete. Fluorescence spectra were measured using a Fluoro Sens 9003 Fluorescence Spectrophotometer. Fluorescent microscope images of HepG-2 cells were taken on DM5000B (Leica, Germany), Co-staining fluorescent microscope images of HepG-2 cells were taken on IX71 (Leica, Germany). All the samples were prepared according to the standard methods.

View Article Online
DOI: 10.1039/C7TB02390E

Cytotoxicity. The cytotoxicity test was performed with HepG-2 human Hepatic cancer cells. **TPA-PP**, **TPA-PPA-1**, **TPA-PPA-2** and **TPA-PPA-3** were sterilized with ultraviolet light and dissolved in DMSO. Then, the solution was diluted with PBS buffer (pH = 7.4) to different concentrations (0, 10, 20, 30, 40 and 50 μg/mL). To obtain complete cell culture medium, 10% PBS, 100 units mL^{-1} penicillin, and 100 units mL^{-1} streptomycin were added in the mixture. HepG-2 human Hepatic cancer cells (purchased from Gansu Provincial Cancer Hospital, Gansu, China) were cultured in the conditioned medium at 37 °C in a humidified environment of 95% O_2 and 5% CO_2. After 96 h of incubation, cell viability was determined by the 3-(4, 5-dimethylthiazol-2-yl)-2, 5-diphenyltetrazolium bromide (MTT) method.

Cell fluorescence imaging. Living human Hepatic cancer (HepG-2) cells (1.0 × 105/well) were cultured overnight and then stained in a Petri dish at 50% confluence with **TPA-PP**, **TPA-PPA-1**, **TPA-PPA-2** and **TPA-PPA-3** solution (20 μg/mL). An image was taken after 1 h incubation,

Live cell counterstain with DAPI. Cells were first stained in the desired concentration by following the previous staining procedure. Cells were then incubated at 37 °C in 5% CO_2 for 12 h and imaged at ambient temperature in the medium. The imaging of DAPI counterstain followed the similar procedure. The final concentration of DAPI was 5 mM. Prior to imaging, the cells were rinsed by fresh medium twice after 10 min of incubation with DAPI.

Synthesis and characterization of TPA-PP, TPA-PPA-1, TPA-PPA-2 and TPA-PPA-3.

Synthesis and characterization of TPA-PP. 4-bromotriphenylamine (4 mmol, 324 g/mol, 1.296 g), pyridine-4-boronic acid (4.2 mmol 215 g/mol, 0.903 g), potassium carbonate (4 mmol 138 g/mol, 0.552 g) and tetrakis(triphenylphosphine)palladium(0) (0.2 mmol, 1155 g/mol, 5% equiv 0.231 g) were dissolved in the mixture of THF (30 mL) and MeOH (30 mL). And then the mixture was refluxed at 120 °C for 48 h under N_2 atmosphere. The reaction mixture was concentrated by rotary evaporation. Then, the N,N-diphenyl-4-(pyridin-4-yl)aniline purified by column chromatography on silica gel (300-400 mesh) with a mixture of petroleum ether and ethyl acetate as eluent (10:1 by volume), obtaining a white solid (1.1 g, 3.32 mmol, 83% yield). Then, the white solid (2 mmol, 322 g/mol, 0.644 g), benzyl bromide (2 mmol, 171 g/mol, 0.342 g) and THF (50 mL), were introduced into a clean round-bottom flask with a magnetic stirrer. Subsequently, the mixture was stirred at 90 °C for 48 h. After

View Article Online
DOI: 10.1039/C7TB02709E

then, the reaction mixture was precipitated from THF, and washed using diethyl ether for several times. An orange powder was obtained by filtration, and dried under vacuum at room temperature overnight. **TPA-PP** was an orange solid (0.747 g, 75% yield). (Scheme S1, Figure S1, ESI†) ^{1}H NMR (600 MHz, DMSO-d_6) δ (TMS, ppm): δ 9.05 (s, 2H), 8.35 (s, 2H), 7.97 (s, 2H), 7.53 (d, J = 6.8 Hz, 2H), 7.44 (s, 1H), 7.42 (d, J = 1.6 Hz, 2H), 7.40 (d, J = 7.7 Hz, 4H), 7.21 (t, J = 7.4 Hz, 2H), 7.17 (d, J = 7.6 Hz, 4H), 6.94 (s, 2H), 5.75 (s, 2H). ^{13}C NMR (150 MHz, DMSO- d_6) δ (TMS, ppm): δ 154.47, 151.72, 146.00, 144.64, 135.11, 130.46, 130.13, 129.65, 129.05, 126.58, 125.80, 124.66, 123.31, 119.85, 62.37.

Synthesis and characterization of TPA-PPA-1. 4-bromotriphenylamine (4 mmol, 324 g/mol, 1.296 g), pyridine-4-boronic acid (4.2 mmol, 215 g/mol, 0.903 g), potassium carbonate (4 mmol, 138 g/mol, 0.552 g) and tetrakis(triphenylphosphine)palladium(0) (0.2 mmol, 1155 g/mol, 5% equ., 0.231 g) were dissolved in the mixture of THF (30 mL) and MeOH (30 mL). And then the mixture was refluxed at 120 °C for 48 h under N_2 atmosphere. The reaction mixture was concentrated by rotary evaporation. Then, the N,N-diphenyl-4-(pyridin-4-yl)aniline purified by column chromatography on silica gel (300-400 mesh) with a mixture of petroleum ether and ethyl acetate as eluent (10:1 by volume), obtaining a white solid (1.1 g, 3.32 mmol, 83% yield). Then, the white solid (2 mmol, 322 g/mol, 0.644 g), 4-bromomethylphenylboronic acid (2 mmol, 213 g/mol, 0.426 g) and THF (50 mL), were introduced into a clean round-bottom flask with a magnetic stirrer. Subsequently, the mixture was stirred at 90 °C for 48 h. After then, the reaction mixture was precipitated from THF, and washed using diethyl ether for several times. A yellow solid powder was obtained by filtration, and dried under vacuum at room temperature overnight. **TPA-PPA-1** was a yellow solid (0.890 g, 87% yield). (Scheme S1, Figure S2, ESI†) ^{1}H NMR (600 MHz, DMSO-d_6) δ (TMS, ppm): δ 9.03 (d, J = 6.9 Hz, 2H), 8.35 (d, J = 7.0 Hz, 2H), 7.96 (d, J = 8.9 Hz, 2H), 7.82 (d, J = 8.0 Hz, 2H), 7.45 (d, J = 7.9 Hz, 2H), 7.40 (d, J = 7.9 Hz, 4H), 7.21 (t, J = 7.4 Hz, 2H), 7.17 (d, J = 7.6 Hz, 4H), 6.93 (d, J = 8.9 Hz, 2H), 5.74 (s, 2H). ^{13}C NMR (150 MHz, DMSO-d_6) δ (TMS, ppm): δ 154.45, 151.72, 146.00, 144.69, 136.69, 135.27, 130.46, 130.13, 127.93, 126.57, 125.75, 124.66, 123.28, 119.86, 62.36.

Synthesis and characterization of TPA-PPA-2. Bis(4-bromophenyl)amine (3 mmol, 326 g/mol, 0.978 g), iodobenzene (3.3 mmol, 203 g/mol, 0.609 g), 1,10-phenanthroline (0.9 mmol, 198 g/mol, 0.178 g), CuI (0.3 mmol, 190 g/mol, 0.057 g), and potassium hydroxide (3 mmol, 56 g/mol, 0.168 g) were introduced to a 100 mL round-bottomed flask containing 60 mL of toluene under N_2 atmosphere. The reaction mixture was rapidly heated to the reflux temperature of 120 °C for 3 h. Then, the reaction mixture was cooled to 75 °C and extracted by 200 mL of toluene and 150 mL of deionized water, respectively. And the organic phase was decolorized by activated carbon. The adsorbents were removed by hot filtration, and the solvent was removed by rotary evaporation. The product was subjected to further purified by column chromatography on silica gel (300-400 mesh) with a mixture of petroleum ether and ethyl acetate as eluent (5:1 by volume), obtaining a white solid (0.916 g, 76% yield). Then, the white solid (2 mmol, 402 g/mol, 0.804 g) was reacted with pyridine-4-boronic acid (4.4 mmol, 215 g/mol, 0.946 g) through Suzuki reaction. Therefore, the pure product was obtained (0.630 g, 79% yield). Finally, it was reacted with 4-bromomethylphenylboronic acid through salt-forming reaction. Reaction condition was similar to Synthesis of **TPA-PP**. **TPA-PPA-2** was an orange solid (0.721 g, 87% yield). (Scheme S2, Figure S3, ESI†) ^{1}H NMR (600 MHz, DMSO-d_6) δ (TMS, ppm): δ 9.23 – 9.04 (m, 4H), 8.53 - 8.39 (m, 4H), 8.14 (d, J = 18.1 Hz, 4H), 8.09 (t, J = 8.8 Hz, 4H), 7.84 (t, J = 7.0 Hz, 4H), 7.49 (d, J = 8.7 Hz, 4H), 7.48 - 7.40 (m, 2H), 7.33 (d, J = 12.9, 5.5 Hz, 1H), 7.27 (d, J = 6.2, 4.1 Hz, 2H), 7.22 (d, J = 8.8 Hz, 4H), 5.94 – 5.60 (m, 4H). ^{13}C NMR (150 MHz, DMSO-d_6) δ (TMS, ppm): δ 154.36, 150.24, 144.96, 136.61, 135.27, 130.80, 130.33, 128.97, 127.97, 127.36, 126.95, 124.11, 123.48, 121.56, 116.31, 62.59.

Synthesis and characterization of TPA-PPA-3. Tris(4-iodophenyl)amine (2 mmol, 623 g/mol, 1.246 g), pyridine-4-boronic acid (6.3 mmol, 215 g/mol, 1.354 g), potassium carbonate (6 mmol, 138 g/mol, 0.828 g) and tetrakis(triphenylphosphine)palladium(0) (0.3 mmol, 1155 g/mol, 5% equiv, 0.346 g) were dissolved in the mixture of THF (30 mL) and MeOH (30 mL). And then the mixture was refluxed at 120 °C for 48 h under N_2 atmosphere. The reaction mixture was concentrated by rotary evaporation. Then, the crude product purified by column chromatography on silica gel (300-400 mesh) with a mixture of petroleum ether and ethyl acetate as eluent (1:1 by volume), obtaining a white solid (0.599 g, 63% yield). Then, the white solid (1 mmol, 476 g/mol, 0.476 g), 4-bromomethylphenylboronic acid (3 mmol, 213 g/mol, 0.629 g) and THF (50 mL), were introduced into a clean round-bottom flask with a magnetic stirrer. Subsequently, the mixture was stirred at 90 °C for 48 h. After then, the reaction mixture was precipitated from THF, and washed using diethyl ether for several times. An orange powder was obtained by filtration, and dried under vacuum at room temperature overnight. **TPA-PPA-3** was an orange solid (0.953 g, 85% yield). (Scheme S3, Figure S4, ESI†) ^{1}H NMR (600 MHz, DMSO-d_6) δ (TMS, ppm): δ 9.16 (d, J = 6.9 Hz, 6H), 8.49 (d, J = 6.9 Hz, 6H), 8.12 (d, J = 8.5 Hz, 6H), 8.12 (s, 1H), 7.83 (d, J = 7.8 Hz, 6H), 7.48 (d, J = 4.7 Hz, 6H), 7.31 (d, J = 11.6 Hz, 6H), 5.81 (d, J = 9.1 Hz, 6H). ^{13}C NMR (150 MHz, DMSO-d_6) δ (TMS, ppm): δ 154.33, 149.90, 145.02, 136.60, 135.28, 130.46, 129.24, 127.98, 125.32, 124.53, 124.32, 62.64.

Acknowledgements

This work is supported by the National Natural Science Foundation of China (No. 21764012).

Notes and references

1 (a) A. Patel, L. Malinovska,; S. Saha, J. Wang, S. Alberti, Y. Krishnan, A. A. Hyman, *Science*, 2017, 356, 753; (b) S. Lee, K. K. Yuen, K. A. Jolliffe, J. Yoon, *Chem. Soc. Rev.*, 2015, 44, 1749; (c)

X. Li, X. Guo, L. Cao, Z. Xun, S. Wang, S. Li, G. Yang, *Angew. Chem. Int. Ed.*, 2014, 53, 7809; (d) D. Cheng, Y. Li, J. Wang, Y. Sun, L. Jin, C. Li, Y. Lu, *Chem. Commun.*, 2015, 51, 8544.

2 (a) S. Biswas, K. Kinbara, T. Niwa, H. Taguchi, N. Ishii, S. Watanabe, T. Aida, *Nat. chem.*, 2013, 5, 613; (b) M. M. Gottesman, T. Fojo, S. E. Bates, *Nat. Rev. Cancer*, 2002, 2, 48; (c) A. V. Gourine, E. Llaudet, N. Dale, K. M. Spyer, *Nature*, 2005, 436, 108.

3 (a) S. Biswas, K. Kinbara, T. Niwa, H. Taguchi, N. Ishii, S. Watanabe, T. Aida, *Nat. Chem.*, 2013, 5, 613; (b) D. G. Hardie, F. A. Ross, S. A. Hawley, *Nat. rev. Mol. cell bio.*, 2012. 13, 251; (c) G. Burnstock, *Trends in pharmacological sci.*, 2006, 27, 166; (d) F. M. Ashcroft, F. M. Gribble, *Diabetologia*, 1999, 42, 903.

4 (a) N. Li, J. X. Wu, D. Ding, J. Cheng, N. Gao, L. Chen, *Cell*, 2017, 168, 101-110; (b) X. Wang, S. Arai, X. Song, D. Reichart, K. Du, G. Pascual, R. Kurokawa, *Nature*, 2008, 454, 126.

5 (a) M. T. Lin, M. F. Beal, *Nature*, 2006, 443, 787; (b) D. H. Lee, S. Y. Kim, J. I. Hong, *Angew. Chem. Int. Ed.*, 2004, 43, 4777.

6 (a) W. Xu, Z. Zeng, J. H. Jiang, Y. T. Chang, L. Yuan, *Angew. Chem. Int. Ed.*, 2016, 55, 13658; (b) J. Deng, K. Wang, M. Wang, P. Yu, L. Mao, *J. Am. Chem. Soc.*, 2017, 139, 5877; (c) L. Wang, L. Yuan, X. Zeng, J. Peng, Y. Ni, J. C. Er, Y. T. Chang, *Angew. Chem. Int. Ed.*, 2016, 55, 1773; (d) N. Jiang, J. Fan, F. Xu, X. Peng, H. Mu, J. Wang, X. Xiong, *Angew. Chem. Int. Ed.*, 2015, 54, 2510; (e) Y. Yang, X. Wang, Q. Cui, Q. Cao, L. Li, *ACS Appl. Mater. Inter.*, 2016, 8, 7440; (f) M. Zhang, G. Feng, Z. Song, Y. P. Zhou, H. Y. Chao, D. Yuan, B. Liu, *J. Am. Chem. Soc.*, 2014, 136, 7241; (g) M. endrell, D. Zhai, J. C. Er, Y. T. Chang, *Chem. Rev.*, 2012, 112, 4391.

7 X. Li, X. Guo, L. Cao, Z. Xun, S. Wang, S. Li, G. Yang, *Angew. Chem. Int. Ed.*, 2014, 53, 7809.

8 (a) Z. Chen, P. Wu, R. Cong, N. Xu, Y. Tan, C. Tan, Y. Jiang, *ACS Appl. Mater. Inter.*, 2015, 8, 3567. (b) F. Li, C. Li, X. Liu, Y. Chen, T. Bai, L. Wang, S. Feng, *Chem.- Eur. J.*, 2012, 18, 11641-11646.

9 S. Nakano, M. Fukuda, T. Tamura, R. Sakaguchi, E. Nakata, T. Morii, *J. Am. Chem. Soc.*, 2013, 135, 3465

10 Z. Xu, N. J. Singh, J. Lim, J. Pan, H. N. Kim, S. Park, J. Yoon, *J. Am. Chem. Soc.*, 2009, 131, 15528.

11 (a) A. S. Rao, D. Kim, H. Nam, H. Jo, K. H. Kim, C. Ban, K. H Ahn, *Chem. Commun.*, 2012, 48, 3206; (b) J. Lai, B. P. Shah, Y. Zhang, L. Yang, K. B. Lee, *ACS nano*, 2015, 9, 5234; (c) Q. Cui, Y. Yang, C. Yao, R. Liu, L. Li, *ACS Appl. Mater. Inter.*, 2016, 8, 35578.

12 J. H. Zhu, C. Yu, Y. Chen, J. Shin, Q. Y. Cao, J. S. Kim, *Chem. Commun.*, 2017, 53, 4342.

13 (a) K. Okuro, M. Sasaki, T. Aida, *J. Am. Chem. Soc.,* **2016**, 138, 5527; (b) A. J. Moro, P. J. Cywinski, S. Körsten, G. J. Mohr, *Chem. Commun.*, 2010, 46, 1085; (c) J. J. Yan, Z. K. Wang, X. S. Lin, C. Y. Hong, H. J. Liang, C. Y. Pan, Y. Z. You, *Adv. Mater.*, 2012, 24, 5617; (d) C. Li, M. Numata, M. Takeuchi, S. Shinkai, *Angew. Chem. Int. Ed.*, 2005, 44, 6371.

14 H. C. Ma, Z. M. Yang, H. Y. Cao, L. Lei, L. Chang, Y. C. Ma, Z. Q. Lei, J. *Mater. Chem. B,* 2017, 5, 655.

15 H. Zhu, J. Fan, J. Du, X. Peng, *Acc. Chem. Res*., 2016, 49, 2115.

16 (a) L. Wang, L. Yuan, X. Zeng, J. Peng, Y. Ni, J. C. Er, Y. T. Chang, *Angew. Chem. Int. Ed.*, 2016, 55, 1773; (b) Y. Kanekiyo, R. Naganawa, H. Tao, *Chem. Commun.*, 2004, 1006; (c) Y. Liu, C. Deng, L. Tang, A. Qin, R. Hu, J. Z. Sun, B. Z. Tang, *J. Am. Chem. Soc.*, 2010, 133, 660.

17 Y. Ooyama, S. Inoue, T. Nagano, K. Kushimoto, J. Ohshita, I. Imae, Y. Harima, *Angew. Chem.*, 2011, 123, 7567.

18 Z. Yang, W. Qin, J. W. Lam, S. Chen, H. H. Sung, I. D. Williams, B. Z. Tang, *Chem. Sci.*, 2013, 4, 3725.

19 Y. Hong, H. Xiong, J. W. Y. Lam, M. Häußler, J. Liu, Y. Yu, B. Z. Tang, *Chem. Eur. J.*, 2010, 16, 1232.

20 (a) F. Li, C. Li, X. Liu, T. Bai, W. Dong, X. Zhang, S. Feng, *Dalton Transactions*, 2013, 42, 2015. (b) C. Li, F. Li, T. Li, T. Bai, L. Wang, Z. Shi, S. Feng, *Dalton Transactions*, 2012, 41, 4890.

21 (a) Z. Ning, Z. Chen, Q. Zhang, Y. Yan, S. Qian, Y. Cao, H. Tian, *Adv. Funct. Mater.*, 2007, 17, 3799; (b) Y. Hong, J. W. Lam, B. Z. Tang, *Chem. Soc. Rev.*, 2011, 40, 5361

22 (a) X. Li, X. Zhang, Z. Chi, X. Chao, X. Zhou, Y. Zhang, J. Xu, *Analytical Methods*, 2012, 4, 3338. (b) X. Q. Zhang, X. Y. Zhang, L. Tao, Z. Chi, , J. Xu, Y. Wei, *J. Mater. Chem. B*, 2014, 2, 4398.

23 F. Li, C. Li, J. Liu, X. Liu, L. Zhao, T. Bai, S. Feng, *Nanoscale*, 2013, 5(15), 6950.